Integrative Biology

Predicting cancer cell invasion by single-cell physical phenotyping

Journal:	*Integrative Biology*
Manuscript ID	IB-ART-12-2017-000222.R1
Article Type:	Paper
Date Submitted by the Author:	09-Mar-2018
Complete List of Authors:	Nyberg, Kendra; University of California Los Angeles, Integrative Biology and Physiology; University of California Los Angeles, Bioengineering Bruce, Samuel; University of California Los Angeles, Integrative Biology and Physiology Nguyen, Angelyn; University of California, Los Angeles, Integrative Biology and Physiology Chan, Clara; University of California Los Angeles, Integrative Biology and Physiology Gill, Navjot; University of California Los Angeles, Integrative Biology and Physiology Kim, Tae-Hyung; University of California Los Angeles, Integrative Biology and Physiology; University of California Los Angeles, Semel Institute for Neuroscience and Human Behavior Sloan, Erica; University of California Los Angeles, Semel Institute for Neuroscience and Human Behavior; Monash University, Drug Discovery Biology Theme, Monash Institute of Pharmaceutical Sciences; Peter MacCallum Cancer Institute, Division of Cancer Surgery; University of California Los Angeles, UCLA AIDS Institute Rowat, Amy; University of California Los Angeles, Integrative Biology and Physiology; University of California Los Angeles, Bioengineering; University of California Los Angeles, UCLA Jonsson Comprehensive Cancer Center

Insight, Innovation and Integration

Understanding how the physical phenotypes of cells – such as their deformability and size – are associated with cancer cell invasion would provide insights into mechanisms of invasion, and could also enable physical phenotypes to be used as a label-free biomarker for invasion. However, physical phenotyping measurements have been limited due to challenges in measurement throughput. Here, we use the high throughput quantitative deformability cytometry (q-DC) technology that we recently developed to rapidly measure physical phenotypes of across 19 distinct samples of human breast, ovarian, and pancreatic cancer cell lines. Using the data to train a machine learning algorithm, we develop the physical phenotyping model for invasion, which enables us to predict the invasion of cancer cell lines. More broadly, this methodology provides a framework for predicting functional behavior of cells based on physical phenotypes.

Predicting cancer cell invasion by single-cell physical phenotyping

Kendra D. Nyberg[1,2], Samuel L. Bruce[1], Angelyn V. Nguyen[1], Clara K. Chan[1], Navjot K. Gill[1], Tae-Hyung Kim[1,3], Erica K. Sloan[3-7], Amy C. Rowat[1,2,6,*]

[1]Department of Integrative Biology and Physiology, University of California, Los Angeles, USA.
[2]Department of Bioengineering, University of California, Los Angeles, USA
[3]Semel Institute for Neuroscience and Human Behavior, University of California, Los Angeles, USA.
[4]Drug Discovery Biology Theme, Monash Institute of Pharmaceutical Sciences, Monash University, Parkville, Victoria, Australia.
[5]Division of Cancer Surgery, Peter MacCallum Cancer Centre, Melbourne, Victoria, Australia.
[6]UCLA Jonsson Comprehensive Cancer Center, University of California, Los Angeles, USA.
[7]UCLA AIDS Institute, University of California, Los Angeles, USA.

Corresponding Author*:
Amy C. Rowat, Ph.D.
610 Charles E. Young Dr. East
Los Angeles, CA 90095
Phone: (310)825-4026
Email: rowat@ucla.edu

Author emails: knyberg@ucla.edu, samuelbruce24@gmail.com, angelynnguyen@ucla.edu, clarachan27@gmail.com, navgill@ucla.edu, taehyung.kim@ucla.edu, erica.sloan@monash.edu, rowat@ucla.edu.

ABSTRACT

The physical properties of cells are promising biomarkers for cancer diagnosis and prognosis. Here we determine the physical phenotypes that best distinguish human cancer cell lines, and their relationship to cell invasion. We use the high throughput, single-cell microfluidic method, quantitative deformability cytometry (q-DC), to measure six physical phenotypes including elastic modulus, cell fluidity, transit time, entry time, cell size, and maximum strain at rates of 10^2 cells/s. By training a k-nearest neighbor machine learning algorithm, we demonstrate that multiparameter analysis of physical phenotypes enhances the accuracy of classifying cancer cell lines compared to single parameters alone. We also discover a set of four physical phenotypes that predict invasion; using these four parameters, we generate the physical phenotype model of invasion by training a multiple linear regression model with experimental data from a set of human ovarian cancer cells that overexpress a panel of tumor suppressor microRNAs. We validate the model by predicting invasion based on measured physical phenotypes of breast and ovarian human cancer cell lines that are subject to genetic or pharmacologic perturbations. Taken together, our results highlight how physical phenotypes of single cells provide a biomarker to predict the invasion of cancer cells.

KEYWORDS

Physical phenotyping, cancer invasion, mechanotype, machine learning, cell classification.

INTRODUCTION

Predicting disease and treatment outcomes based on single-cell phenotypes is critical in medicine from cancer diagnosis to stem cell therapies. In clinical oncology and immunology, single-cell analysis of protein markers and DNA content using flow cytometry is valuable in diagnosis, prognosis, and monitoring patient response to therapy (1). Yet pathological and physiological changes can also manifest as altered cell physical phenotypes, including cell and nuclear size, stiffness, and viscosity. For example, grading of tumor biopsies based on nuclear morphology is widely used for cancer prognosis (2–4). The deformability of cancer cells is also emerging as a convenient biomarker as more invasive cancer cells have altered deformability compared to less invasive cells (5–17). Since cellular physical phenotypes, such as deformability, are inherent properties of cells, they can be rapidly measured without the use of fluorescent markers or labeling agents (18). However, the utility of cell deformability in predicting the invasion of cancer cells remains unclear: many studies show that more invasive cancer cells tend to be more compliant than less invasive or benign cells (5–12); but there are also contexts where more invasive cells are found to be stiffer (13–17). These contrasting findings suggest that the invasion of cancer cells cannot be universally predicted based on cell deformability, and incite studies into which additional physical phenotypes may collectively predict invasion.

Microfluidic methods are especially valuable for physical phenotyping, as they enable rapid measurements of single cells. One such method is transit-based deformability cytometry, which probes physiologically-relevant deformations of cells through narrow gaps across varying deformation time and length scales (10,19–22). While transit time T_T is a relative measurement, this parameter can distinguish cancer cell lines from benign cells (10,21). However, it is challenging to compare common metrics of cell physical phenotypes, such as deformability and transit time, across experiments because such measurements are not typically calibrated (23). We recently developed the quantitative deformability cytometry (q-DC) method, which uses calibration particles and power law rheology to obtain calibrated single-cell measurements of elastic modulus E and fluidity β, as well as four additional physical phenotypes (24). Performing such calibrated measurements across studies enables comparisons across cell types that can address how multiple cell physical phenotypes can be leveraged to predict cell invasion.

Using multiple features of clinical samples to train machine learning algorithms is showing value in diagnosis and predicting disease outcomes (25–33). Since physical phenotypes are inherent properties of cells, such measurements can provide a low-cost way to increase the feature space for machine learning algorithms and to generate more robust models. For example, biophysical signatures of mesenchymal stromal cells can predict their regenerative capability *in vivo* as indicated by ectopic bone formation in mouse models (34). Analysis of sets of physical phenotypes also improves the classification of stem cells and their progenitors as demonstrated by studies using atomic force microscopy (AFM) (34–40), cross-slot deformability cytometry (41), and optofluidic time-stretch microscopy (42). Thus, we hypothesized that multiparameter physical phenotyping could be used to train a machine learning algorithm to predict the invasion of cancer cells.

Here we use calibrated, physical phenotype measurements obtained by q-DC to predict the invasion of human cancer cell lines. We perform multiparameter analysis of six physical phenotypes for eleven different cancer cell lines with eight genetic or pharmacologic perturbations, resulting in nineteen distinct cell samples. To measure the physical phenotypes of

single cells, we use quantitative deformability cytometry (q-DC) to obtain calibrated measurements of elastic modulus E and cell fluidity β, as well as transit time T_T, entry time T_E, cell size D_{cell}, and maximum strain ϵ_{max}, at rates of 10^2 cells/s (24). We show that multiparameter analysis of these physical phenotypes can enhance classification of cancer cell lines. From measurements across well-established pancreatic cancer cell lines as well as ovarian cancer cells that overexpress tumor-suppressor microRNAs, we build the predictive physical phenotyping model for invasion, which we validate using both genetic and pharmacologic perturbations of cancer cells. Our results demonstrate the value of rapid physical phenotyping for predicting invasion.

MATERIALS AND METHODS

Cell culture. Nontransformed human pancreatic ductal epithelial (HPDE) cells are obtained from Dr. Ming-Sound Tsao (University Health Network-Princess Margaret Hospital, Canada and University of Toronto, Canada). HPDE cells are cultured in Keratinocyte-SFM medium supplemented with prequalified human recombinant Epidermal Growth Factor 1-53, Bovine Pituitary Extract, and 1% penicillin-streptomycin. The human pancreatic ductal adenocarcinoma (PDAC) cell lines (AsPC-1, Hs766T, MIA PaCa-2, and PANC-1) are from the American Type Culture Collection (ATCC). AsPC-1, Hs766T, MIA PaCa-2 and PANC-1 cells are grown in high glucose, L-glutamine without sodium pyruvate DMEM medium with 10% heat-inactivated fetal bovine serum and 1% penicillin-streptomycin. Fetal bovine serum and penicillin-streptomycin are from Gemini BioProducts, West Sacramento, CA. All cell media and additional media supplements are from Thermo Fisher Scientific Inc., Canoga Park, CA. To test the effects of microRNAs that are associated with improved patient survival (43), we overexpress microRNA mimics (microRNA-508-3p, microRNA-508-5p, microRNA-509-3p, microRNA-509-5p and microRNA-130b-3p) in human ovarian cancer (HEYA8) cells; microRNA mimics, mock, and scrambled (SCR) negative controls are from Dr. Preethi Gunaratne (University of Houston, USA) (43,44). HEYA8 cells are cultured in RPMI 1640 medium supplemented with 10% fetal bovine serum and 1% of penicillin-streptomycin. Cells are transiently transfected at 24 nM using Lipofectamine 2000 in serum-free OptiMEM medium, followed by the addition of 10% fetal bovine serum after 4 hours in serum-free conditions. All assays are performed 72 hours post transfection. Human ovarian cancer (OVCA433-GFP, OVCA433-Snail) cells are from Dr. Ruprecht Wiedemeyer (Cedars-Sinai Medical Center, USA) (45). OVCA433 cells are cultured in DMEM medium with L-Glutamine, Glucose, and Sodium Pyruvate. Medium is supplemented with 10% fetal bovine serum, 1% Anti-anti, and 2.5 µg/ml Plasmocin Prophylactic with 5 µg/ml blasticidin S HCl.

A highly metastatic variant of MDA-MB-231 cells (MDA-MB-231-HM, gift from Dr. Zhou Ou, Fudan University Shanghai Cancer Center, China)(46) is cultivated in DMEM medium with L-Glutamine, Glucose, and Sodium Pyruvate, supplemented with 10% fetal bovine serum and 1% penicillin-streptomycin. The agonist (isoproterenol) for the β-adrenergic receptor is from Sigma-Aldrich (St. Louis, MO). Cells are treated for 24 hours prior to measurements.

All cells are cultured at 37^{o}C with 5% CO_2. Cell line authentication is performed using short tandem repeat (STR) profiling (Laragen Inc., Culver City, CA, USA and CellBank Australia, Westmead, NSW, Australia). Prior to deformability measurements, 0.01% (v/v) Pluronic F-127 surfactant (Sigma-Aldrich, St. Louis, MO, USA) is added to the cell suspension to reduce cell

adhesion to the PDMS walls. While F-127 treatment does not significantly affect E values of suspended cells (24), we observe a significant decrease in cell-to-PDMS adhesion in some cell types such as HPDE cells (23).

Microfluidic chip fabrication. Negative photomasks are designed in AutoCAD (Autodesk, Inc., San Rafael, CA) and printed on chrome by the Nanolab at UCLA. The design of the q-DC devices is described previously (23). Silicone masters are fabricated using soft photolithography techniques (47). Polydimethylsiloxane (PDMS) (Sylgard Dow Corning, Midland, MI, USA) with a 10:1 w/w ratio of base and curing agent is poured onto the master wafer and placed under vacuum to degas for 1 hour. To cure the PDMS, the wafer and PDMS mixture is placed in a 65^{o}C oven for 2 hours. Inlets and outlets are created using a biopsy punch with a 0.75 mm bore size (Sigma-Aldrich, St. Louis, MO, USA). The devices are then bonded to coverglass (#1.5 thickness) by plasma and baked at 80^{o}C for 5 minutes to facilitate bonding. To ensure consistent device surface properties, q-DC experiments are performed 24 h after plasma treatment (23). Under these conditions, PDMS has an elastic modulus on the order of 1 MPa (48). As the typical mechanical stress associated with a cell deforming through the constricted channel is ~ 10 kPa (24), the deformation of the PDMS is minimal while the cell transits through the constriction.

q-DC microfluidic experiment. To measure the physical properties of single cells, we use the q-DC method as previously reported (24). In brief, q-DC microfluidic devices are mounted onto an inverted microscope (Zeiss Observer, Zeiss, Oberkochen, Germany) that is equipped with a 20×/0.40 NA objective. A constant air pressure (69 kPa) drives cell suspensions to flow through the channels. As cells deform through microfluidic constrictions with 10 μm height and 9 μm width, a CMOS camera (MicroRNAcoEx4, Vision Research, Wayne, NJ, USA) is used to capture brightfield images at rates of 600 to 2000 frames per second. For cell suspensions with a density of 2 x 10^6 cells/mL that are driven by an applied pressure of 69 kPa (10 psi), single-cell measurements can be acquired at rates of 10^2 cells/s. While the timescale of the initial cell deformation into microfluidic constrictions is largely determined by cell deformability (49–51), 0.01% (w/v) pluronic F-127 surfactant (Sigma-Aldrich, St. Louis, MO, USA) is added to the cell media to minimize cell-surface interactions.

Measurements of cell physical properties using q-DC. To conduct multiparameter analysis of cell physical properties, the displacement and shape of single cells are tracked using a MATLAB code (Mathworks, Natick, MA, USA; code available online on GitHub) (24). This enables us to acquire cell size D_{cell}, the time required for a cell to deform into the constriction T_E, and the time required for a cell to transit completely through the constriction T_T (24). We also measure the time-dependent strain as $\epsilon(t) = \frac{C_o - C(t)}{C_o}$, where C is the circularity, $C(t) = \frac{4\pi A(t)}{P(t)^2}$. We set the initial circularity value as $C_o = 1$, since the cells exhibit a circularity close to a perfect circle prior to entering the constriction. At the end of the entry time, the cell reaches a minimum circularity and corresponding maximum strain ϵ_{max}.

To extract elastic modulus E and cell fluidity β, we determine the applied stress, $\bar{\sigma}$, during cell deformation using agarose calibration particles with well-characterized Young's moduli. Measuring the stress-strain relationship for the calibration particles enables us to determine the stress as a function of driving pressure in both 9 x 10 μm^2 and 7 x 10 μm^2 device geometries

(24). By fitting a power law rheology model to the time-dependent strain data obtained for individual cells, we can extract elastic modulus E and cell fluidity β:

$$\epsilon(t) = \frac{\bar{\sigma}}{E}\left(\frac{t}{\tau_o}\right)^{\beta}, \qquad \text{Eq. 1}$$

where E is the elastic modulus when $t = \tau$; τ is the characteristic timescale, set to 1 s; and β is the power law exponent, which represents cell fluidity. For purely elastic materials, $\beta = 0$; for purely viscous materials, $\beta = 1$. As elastic modulus E, cell fluidity β, entry time T_E, and transit time T_T depend on cell size, we analyze cells that have D_{cell} that is the population median ± 1 μm.

Classifying cell lines using q-DC. To evaluate the power of q-DC parameters to classify cells, we perform supervised machine learning using the k-nearest neighbor (k-NN) algorithm (S. Fig. 1A). K-NN is a non-parametric algorithm that does not assume the underlying data fits a particular model and is among the simplest machine learning algorithms to conceptualize and execute (25). To implement the k-NN classification algorithm, we first map each cell sample into a multidimensional feature space of physical phenotypes (Fig. 2B). We train the algorithm by considering the k nearest neighbors of individual data points based on their Euclidean distance; the resultant clusters of data have the highest overlap in feature space or the most similar physical signatures. The class assigned to new data points is determined by the most common class of the k number of nearest neighbors in the training set. When selecting the integer, k, there is a tradeoff between overfitting and underfitting (52–54): when k = 1, the class is assigned based on only one closest neighbor in the feature space, and the algorithm is thus subject to noise and overfitting. By contrast, if k is the same size as the sample size, then the class assigned is the most common class in the feature space, and multiple classes cannot be assigned. Here we use k = 10, as it yields similar accuracies compared to k > 3, but spans a greater distance in the feature space to reduce overfitting; k = 10 also ensures that we can identify multiple classes as k is still significantly smaller than the training set of 400 samples per cross validation step (S. Fig. 1B, S. Table. 1).

To implement k-NN, we first log-transform the physical phenotype data as single-cell populations exhibit non-normal distributions. Since training a k-NN algorithm is computationally expensive for large data sets (52), we use the median values of physical phenotypes as a proof-of-concept demonstration. We supply a known set of input data using statistical bootstrapping: for each cell line, we generate a representative training set of median q-DC predictors from 500 subsets of experimental data, which each contain 100 randomly-sampled cells with replacement. To determine classification accuracy, we execute the training and testing with 5-fold cross validation: the data is evenly partitioned into 5 subsets. For each round of cross validation, we combine 4 subsets to generate a training set, and use the fifth subset as the testing set. Classification accuracy is defined as the percentage of correct classifications over total classifications across each of the training sets.

Physical phenotype model of invasion using q-DC. To evaluate if rapid physical phenotyping can predict cancer cell invasion, we build the physical phenotype model of invasion. We perform multiple linear regression using physical phenotype data obtained by q-DC to predict invasion rates that we previously measured using a 3D scratch wound invasion assay (12–14) (MATLAB, Mathworks, Natick, MA, USA) and were previously reported in the literature (55–58). As q-DC

measurements of cell physical phenotypes depend on cell size (Fig. 1E)(24), we bin our data based on the median cell size for each panel ± 1 μm. We perform a log-transform as our data is non-normally distributed. To evaluate linear regression error, we utilize the single-cell q-DC data to train linear regression models using 1000 bootstrapped samples of single-cell physical phenotypes. Each bootstrapped sample generates a linear combination of physical phenotypes to predict invasion and their associated coefficients that minimize residuals. The physical phenotype model is determined by the median coefficient for each parameter. The correlation coefficient between predicted invasion and measured invasion is determined as the average correlation coefficient. Similar to the training analysis, we predict invasion using the physical phenotype model with 1000 bootstrapped samples of the q-DC data of single-cells; this enables us to determine the average predicted invasion. To evaluate the predictive accuracy of the model, we compare the ranking of measured invasion determined from both previous experiments (13,14) and literature (55–58) with the invasion values obtained from the physical phenotyping model for invasion.

RESULTS

Multiparameter physical phenotyping by q-DC. To rapidly measure the physical phenotypes of single cells, we use transit-based deformability cytometry; this method uses a microfluidic device that consists of an array of branching channels (20,22,23,59,60), which lead to micron-scale constrictions (Fig. 1A,B). The timescale for cells to transit through these narrow channels provides a simple measure of cell deformability (Fig. 1B,C): stiffer cells tend to have longer transit times (T_T) compared to more compliant cells (61). To extract additional parameters from transit-based microfluidic measurements, we recently developed quantitative deformability cytometry (q-DC), which enables calibrated single-cell measurements of physical phenotypes including elastic modulus E and fluidity β that are extracted using power law rheology.

We find that a population of single cells exhibits variability in physical phenotypes, as shown in Fig 1B. For this example showing the stiffness E of HPDE cells, we find the interquartile range of E spans 1.2 to 4.2 kPa, and displays a median E of 2.7 kPa, which is consistent with previous measurements by AFM (62). The heterogeneity in physical phenotypes across a population of single cells that we observe may be attributed to cell-to-cell variability in protein expression (63), F-actin organization (64,65), cell cycle stage (66–68), and nuclear-to-cytoplasmic ratio (69).

In addition to E, T_T, and β, we also obtain cell size D_{cell}, from the diameter of the unconstrained cell prior to deformation; maximum strain $\epsilon_{\max}$, based on the minimum circularity that occurs as the cell deforms through the constriction; and entry time T_E, which is the time required for a cell to reach maximum strain (Fig 1B). While q-DC enables measurements of multiple physical phenotypes, it is not clear how this additional information improves the accuracy of cell classification and prediction of invasion over standard measurements of T_T alone.

Pairwise correlation analysis of q-DC parameters. To assess the value of multiple biophysical parameters for classification of different cell types, we use q-DC to measure physical phenotypes of human pancreatic ductal adenocarcinoma (PDAC) cell lines that are derived from primary tumors (PANC-1 and MIA PaCa-2), and secondary sites (AsPC-1 and Hs766T), as well as a non-

transformed human ductal pancreatic epithelial (HPDE) control cell line. These cell lines exhibit distinct differences in invasion (13), and therefore provide a model system for testing q-DC classification of cells.

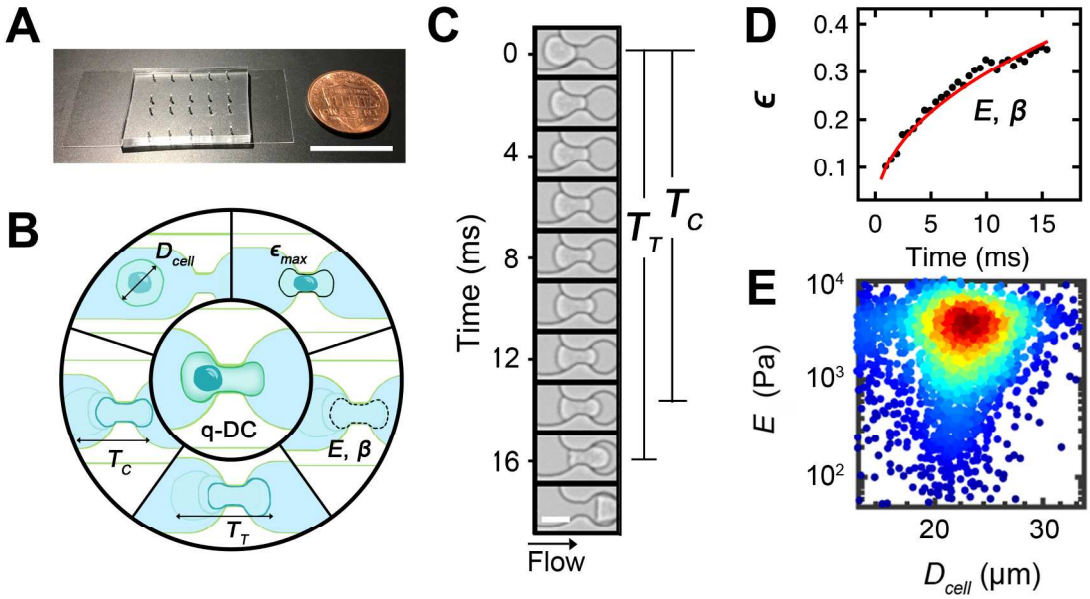

Fig 1. Overview of cell physical phenotyping by quantitative deformability cytometry (q-DC). (*A*) Image of q-DC microfluidic device mounted on a glass coverslip next to an American penny for scale. Scale, 19 mm. (*B*) Schematic overview of physical phenotyping by q-DC. By deforming cells through microfluidic constrictions, we obtain measurements of elastic modulus E, cell fluidity β, transit time T_T, entry time T_E, cell size D_{cell}, and maximum strain ϵ_{max} for individual cells. (*C*) A representative cell deforming through a microfluidic channel of the q-DC device. Entry time T_E is the time required for a cell to reach maximum strain ϵ_{max}; transit time T_T is the time required for the cell to transit through the constriction. Scale bar, 20 μm. (*D*) Black dots represent the strain of the single cell shown in panel *C* as a function of time. Red solid line represents power law fit to single-cell strain trajectory over the entry timescale, T_E. Using power law rheology, we extract elastic modulus, E, and fluidity exponent, β. (*E*) Representative scatter plot of E and D_{cell} for human pancreatic ductal epithelial (HPDE) cells. Each dot represents a single cell and color denotes number density. Shown here are a total of N = 3231 cells.

To identify which physical phenotypes provide unique information for classifying populations of single cells and which ones are statistically redundant, we first evaluate the correlation strength between pairs of the six q-DC outputs, E, β, T_T, T_E, D_{cell}, and ϵ_{max} (S. Fig. 2, S. Table. 2). Spearman's rank correlation coefficients of -1 and +1 reflect pairs of parameters that are highly correlated and statistically dependent on each other. By contrast, correlation coefficients with a low absolute value indicate pairs of parameters that are weakly correlated with each other; each parameter from a weakly correlated pair will more likely provide unique information, as they are more statistically independent from each other.

Analysis of the Spearman's correlation coefficients reveals that T_T and T_E are highly correlated (r = 0.95; p $\ll$ 0.001) (Fig. 1C, S. Fig. 2, S. Table. 2); this is expected as transit time is defined as the time for a cell to enter and exit the constriction. We also find that β and E are strongly correlated (r = -0.77; p $\ll$ 0.001); this scaling of E and β is consistent with the behavior of soft glassy materials (19,70). All other pairwise comparisons between parameters, such as D_{cell} to ϵ_{max}, T_T, E, are weakly correlated with -0.48 < r < 0.64 (S. Table. 2), suggesting that combinations of these parameters could provide unique information for characterizing cell lines.

Multiparameter analysis for classification of pancreatic cells. To assess the value of q-DC data sets in classifying PDAC cell lines, we use the k-nearest neighbors (k-NN) algorithm to classify cell lines based on physical phenotypes. In the k-NN method, training data establishes a multidimensional feature space, where q-DC parameters define each dimension; cell lines are then classified based on the identity of their k nearest neighbors in the pre-established feature space. To evaluate how the number of predictors and combinations thereof affect classification accuracy, we first assess the ability of single physical phenotypes to classify cells. We find that single parameters alone offer low classification accuracy of cell lines: T_T yields 65% accuracy in predicting the correct cell line from our panel of PDAC cell lines, E yields 59% accuracy, and D_{cell} gives 52% (Fig. 2A).

Including additional physical phenotypes significantly enhances classification accuracy: $\{E, T_T\}$ provide a model accuracy of 87% and with $\{T_T, D_{cell}\}$, the model accuracy increases to 91% (Fig. 2A, S. Fig. 3). Other combinations of two parameters yield accuracies ranging from 69% to 89% (S. Fig. 3). Including an additional third parameter further improves accuracy, but with smaller gains: both $\{E, T_T, D_{cell}\}$ and $\{E, \epsilon_{max}, D_{cell}\}$ result in 94% accuracy. The highest accuracy of 96% can be obtained using four parameters $\{E, T_T, D_{cell}, \epsilon_{max}\}$ (Fig. 2A,B). Surprisingly, we find that using additional q-DC parameters does not improve classification accuracy, which ranges from 92% to 96% when using five and six physical phenotypes; this highlights how certain pairs of parameters, such as T_T and T_E, are highly correlated. Therefore, we use $\{E, T_T, D_{cell}, \epsilon_{max}\}$ as a reduced set of parameters, which minimizes cross-correlations and provides the highest classification accuracy with the least amount of parameters.

Since transit time T_T is a common metric for cell deformability that is obtained by transit-based deformability cytometry (22), we next evaluate the benefit of q-DC parameters by comparing the performance of the k-NN algorithm using the reduced set of parameters to T_T alone (Fig. 2C, D). For the k-NN algorithm using T_T as a single predictor, we find the algorithm performs poorly: the true positive rate for each cell line ranges from 0.33 to 0.86 (Fig. 2C). For example, the true positive rate for PANC-1 cells is 0.33, indicating that only 33% of PANC-1 samples are correctly identified as PANC-1 cells, 41% are incorrectly identified as HPDE cells, and 26% as AsPC-1 cells (Fig. 2C). When $\{T_T\}$ is used, the true positive rate averaged across all cell lines is 0.65 and the false positive rate is 0.35. By contrast, the reduced set of q-DC parameters $\{E, T_T, D_{cell}, \epsilon_{max}\}$ significantly improves the average true positive rate to 0.96. For example, the true positive rate for PANC-1 cells is 1.0, where 100% of PANC-1 samples are correctly identified. Additionally, the true positive rate for Hs766T is 0.94, where 94% of Hs766T samples are correctly identified, while 6% are identified as MIA PaCa-2 (Fig. 2D). We also observe the reduced set $\{E, T_T, D_{cell}, \epsilon_{max}\}$ decreases the false positive rate, which ranges from 0 to 0.06 (average = 0.04) (Fig. 2D). Taken together, these findings indicate that q-DC predictors increase the accuracy for classifying PDAC cell lines compared to T_T alone.

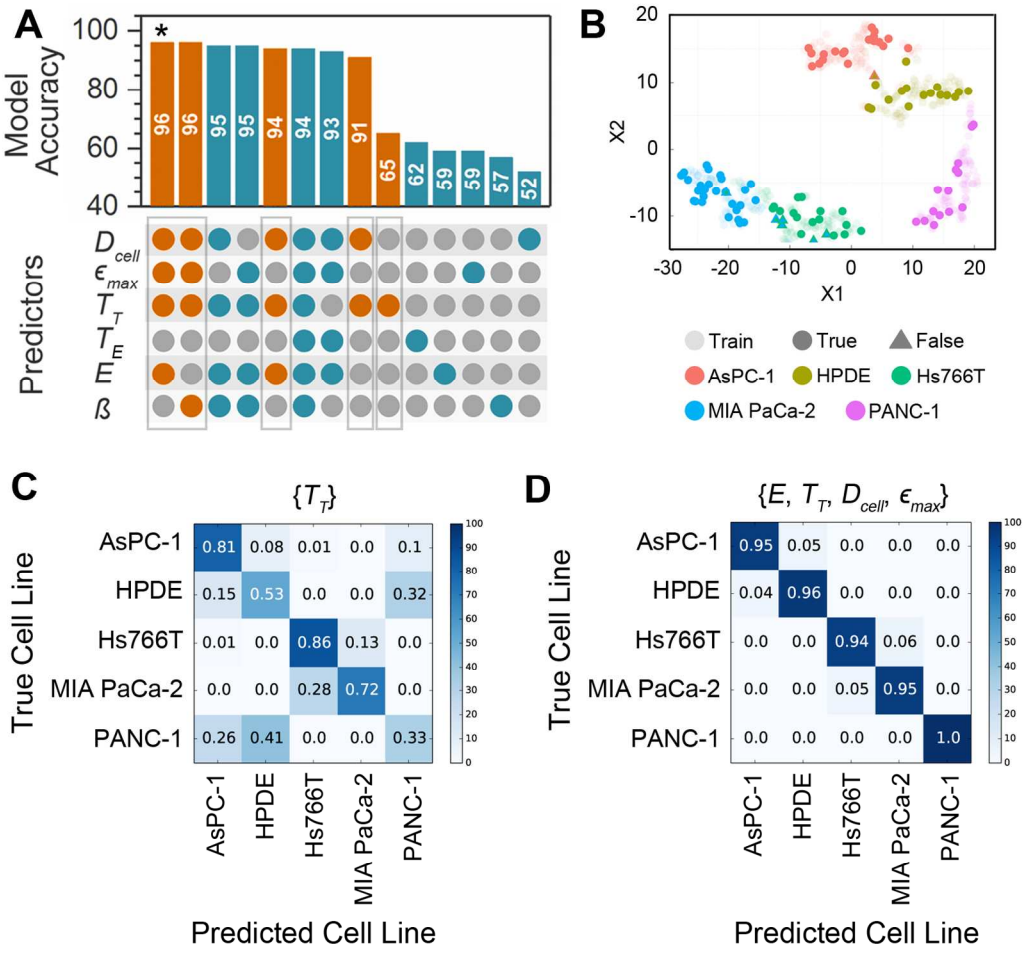

Fig. 2. Predictive power of q-DC outputs for cell classification. (*A*) Accuracy of k-nearest neighbor machine learning algorithm for classifying human pancreatic cell lines. Each bar represents the accuracy of models built with varying combinations of q-DC predictors as indicated by the colored dots; grey dots represent excluded predictors. Orange bars and dots represent the highest accuracy that can be achieved with a set of one, two, three, and four physical phenotypes. Turquoise bars and dots show accuracy obtained by all other combinations of physical phenotypes. Asterisk shows the reduced set of predictors that provides the greatest accuracy with the least number of parameters. White numbers show the accuracy, which is calculated as the percentage of data subsets that are correctly identified as one of the five pancreatic cell lines. S. Fig. 3 illustrates the accuracy of models using additional combinations of q-DC predictors. *(B)* Scatter plot of training and test sets for a single, representative cross-validation step. Data is shown in a visual interactive stochastic neighbor embedding (viSNE) scatter plot (41,71), which projects the reduced set {E, T_T, D_{cell}, ϵ_{max}} data onto a 2D vector space. Transparent markers illustrate the data used in the training set. Opaque markers represent the test set. Circles show samples that are correctly identified (true). Triangles represent samples that are incorrectly classified (false). See S. Fig. 5 for more detailed representation of the

incorrectly classified samples, where the internal color of the triangle represents the true identity and the external color represents the false identity. (C-D) Confusion matrices show the performance of the k-NN algorithm for (C) transit time T_T, and (D) reduced set of q-DC predictors: elastic modulus E, transit time T_T, cell size D_{cell}, and maximum strain ϵ_{max}. Rows represent the true cell line; columns represent the predicted cell line. Color scale denotes the proportion of cells predicted as each cell type.

Relationship of physical phenotypes to cancer cell invasion. To identify which physical phenotypes are the strongest indicators of cancer cell invasion (Fig. 3A), we first evaluate the correlation between invasion and single physical phenotypes of the reduced set, $\{E, T_T, D_{cell}, \epsilon_{max}\}$. Across the panel of PDAC cell lines, we find that individual parameters from the reduced set have poor to moderate correlations with invasion as measured using a 3D scratch wound invasion assay (13,44): Pearson's correlation yields R^2 that range from $R_{D\text{-}Inv}^2 = 0.05 \pm 0.001$ to $R_{E\text{-}Inv}^2 = 0.45 \pm 0.006$ (Fig. 3B). We find the strongest correlation of a single parameter with invasion for E ($R_{E\text{-}Inv}^2 = 0.45 \pm 0.006$), whereby cells that are more invasive tend to have lower E (Fig. 3B). This trend of more invasive cells being more compliant is consistent with previous reports in breast and ovarian cancer cells (5–11). However, the inverse relationship between invasion and E does not hold across all PDAC cell lines as MIA PaCa-2 cells exhibit the lowest elastic modulus yet reduced invasion compared to Hs766T and PANC-1 cells (Fig. 3B).

We also measure the physical phenotype of seven ovarian cancer cell samples that overexpress distinct microRNAs (microRNA-508-3p, microRNA-508-5p, microRNA-509-3p, microRNA-509-5p and microRNA-130b-3p); higher levels of expression of these microRNAs are associated with improved patient survival, as identified through Cancer Genome Atlas (TCGA) data (43). We previously found that microRNA-509-3p, microRNA-509-3p, microRNA-508-3p, and microRNA-130b-3p decrease cell invasion (43,44) and increase cell transit time (44). Physical phenotyping by q-DC reveals that individual phenotypes of microRNA-overexpressing cells also exhibit only moderate correlations to invasion (Fig. 3B). While we find that higher E and T_T are associated with decreased invasion across both established pancreatic cancer cell lines and ovarian cancer cells with manipulated microRNA levels, we find opposite trends for D_{cell} and ϵ_{max} (Fig. 3B); these discrepancies further substantiate the low predictive power of individual physical phenotypes. As single physical phenotypes are not sufficient to predict invasion, we next investigate if multiparameter analysis using the reduced set of four physical phenotypes can collectively predict cancer invasion.

To develop a model that can predict cell invasion on the basis of physical phenotypes, we train a multiple linear regression model using $\{E, T_T, D_{cell}, \epsilon_{max}\}$ and invasion data. While we use data from numerous cell samples, linear regression can be susceptible to overfitting when the number of fitting parameters approaches the number of data points. Therefore, we utilize the data set with the largest number of samples, which is the ovarian cancer cells overexpressing microRNAs that tend to decrease cell invasion (43,44). We account for the number of predictors in the strength of correlation between the measured and predicted invasion using the adjusted-R^2 (R^2_{adj}),

$$R^2_{adj} = 1 - \left[\frac{(1-R^2)(n-1)}{n-m-1}\right], \qquad \text{Eq. 2}$$

where n is the number of observations and m is the number of predictors. For the PDAC cell lines, an R^2_{adj} value does not exist, as there are four fitting parameters in the reduced set and five cell lines. However, building the linear regression model using invasion and physical phenotype data $\{E, T_T, D_{cell}, \epsilon_{max}\}$ from seven ovarian cancer cell lines that overexpress distinct microRNAs results in invasion values that are highly correlated with experimental observations, as indicated by the high $R^2_{adj} = 1.00 \pm 0.002$ (Fig. 3D); we call this multiple linear regression model built with the reduced set of parameters the 'physical phenotype model for invasion'. We also train models with smaller sets of predictors; however, we find that the reduced set of physical phenotypes (E, T_T, D_{cell}, ϵ_{max}) yields the highest R_{adj}^2 value, and thus generates the strongest predictive model with the smallest number of parameters (Fig. 3D).

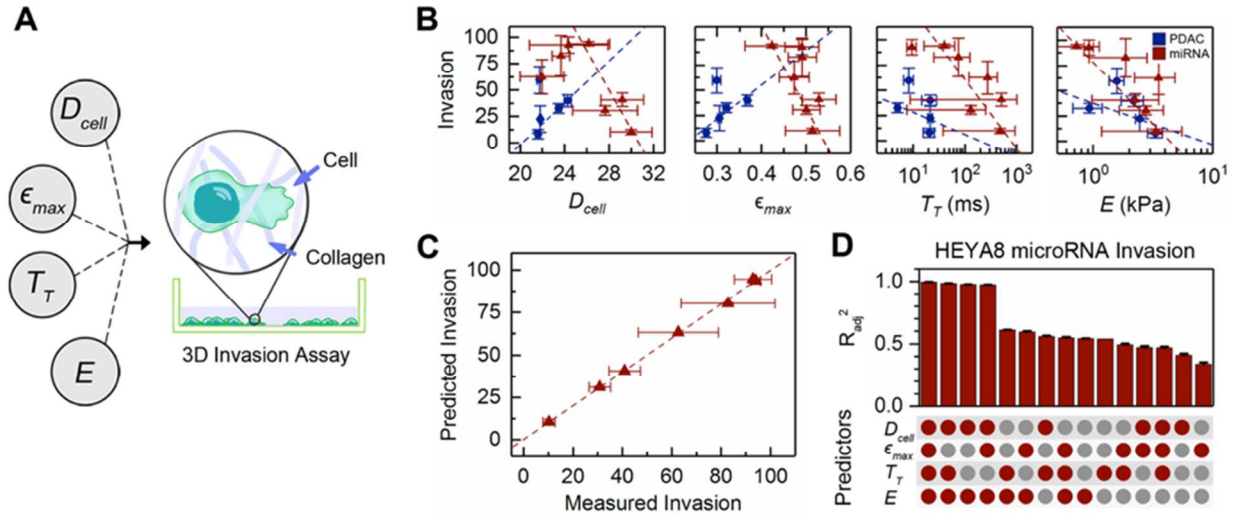

Fig. 3. q-DC parameters as predictors of invasion across cancer cell types. (A) Schematic illustration the reduced set of physical phenotypes, which we use to predict cell invasion, elastic modulus E, transit time T_T, cell size D_{cell}, and maximum strain ϵ_{max}, as measured using 3D invasion assay. (B) Plots showing invasion versus single physical phenotypes for pancreatic adenocarcinoma (PDAC) cell lines (blue circles) and ovarian cancer (HEYA8) cells that overexpress a panel of tumor suppressor microRNAs (red triangles). Each data point represents the median value for a cell sample. Error bars represent standard deviation. Dashed lines show best linear fits. (C) Correlation between measured and predicted invasion using the physical phenotype model for invasion. Dashed lines show best linear fit for the microRNA-overexpressing cells. Data points represent the average value for a cell sample. Error bars represent standard deviation. (D) The strength of correlations between measured and predicted invasion from linear regression models built with combinations of physical phenotypes for microRNA-overexpressing ovarian cancer cells. Colored circles illustrate the set of predictors used in the model. Bars represent adjusted-R^2 (R_{adj}^2) values, which reflect the average strength of the correlation, while accounting for the number of fitting parameters to data points. Error bars represent standard deviation.

Predicting invasion using physical phenotypes. To validate the physical phenotyping model for invasion, we measure physical phenotypes of seven additional cancer cell samples, and

determine how accurately we can predict invasion for samples that are independent of the training set. We first use q-DC to physical phenotype three breast cancer cell lines, MDA-MB-231, MDA-MB-468, and MCF-7 (Fig 4A). These cell lines are well characterized to have varying invasive potentials, from highest to lowest: MDA-MB-231 > MDA-MB-468 > MCF-7 (72,55–58). Other key characteristics of progression are also described for these cell lines, including the propensity to form cell colonies (MDA-MB-231 > MDA-MB-468 > MCF-7) (58). By physical phenotyping using q-DC, we find that MDA-MB-231 cells have decreased E compared to both MDA-MB-468 and MCF-7 cells ($E_{\text{MDA-MB-231}} = 1.2 \pm 0.3$ kPa < $E_{\text{MCF-7}} = 2.0 \pm 0.2$ kPa < $E_{\text{MDA-MB-468}} = 2.7 \pm 0.3$ kPa). Compared to the ranking of invasion of these cells types, we find a weak correlation between E and invasion, which is further quantified by Spearman's correlation coefficient (r = 0.5); these findings support that E alone is not sufficient to predict invasion. We find that transit times follow the same ranking as E, whereby $T_{T\text{ - MDA-MB-231}} = 15 \pm 3$ ms < $T_{T\text{ - MCF-7}} = 25 \pm 5$ ms < $T_{T\text{ – MDA-MB-468}} = 57 \pm 27$ ms (Fig. 4A). Thus, neither E nor T_T is sufficient to predict invasion. However, we discover that the physical phenotyping model for invasion correctly ranks the invasion of these breast cancer cell lines, MDA-MB-231 > MDA-MB-468 > MCF-7 (Fig. 4D). These results further substantiate the power of multiparameter analysis to predict invasion based on physical phenotyping of single cancer cells.

To further validate the physical phenotyping model for invasion, we predict the invasion of ovarian cancer (OVCA433) cells that have been genetically manipulated to generate a pair of epithelial- and mesenchymal-like cell lines. Cancer cells with overexpression of Snail (45) (OVCA433-Snail), a key transcription factor in epithelial-to-mesenchymal transition (EMT) (73) are mesenchymal-like and exhibit increased invasion (73). By contrast, the control cells (OVCA433-GFP) are epithelial-type. Using q-DC to physical phenotype this pair of cell lines, we find that OVCA433-Snail cells have a reduced E compared to the OVCA433-GFP control cells ($E_{\text{OVCA-GFP}} = 1.8 \pm 0.1$ kPa; $E_{\text{OVCA-Snail}} = 1.0 \pm 0.7$ kPa; $p << 0.001$) (Fig 4B). We also observe that OVCA433-Snail cells exhibit shorter transit times than OVCA433-GFP ($T_{T\text{ - OVCA-GFP}} = 22 \pm 2.8$ ms; $T_{T\text{ – OVCA-Snail}} = 16 \pm 1.2$ ms, $p << 0.001$), consistent with the decreased stiffness of the mesenchymal-type OVCA433-Snail cells (Fig. 4B). Using q-DC outputs, we demonstrate that the physical phenotype model for invasion has the power to predict the increased invasion of the OVCA433-Snail cells compared to the control OVCA433-GFP cells (Fig. 4B); these results also demonstrate that physical phenotypes measured by q-DC are consistent with other hallmark characteristics of EMT, such as the increased vimentin to E-cadherin ratio (74) and ability to form cell colonies (75), which are commonly used to define mesenchymal-type cells.

We next assess how increased cell invasion that is caused by pharmacologic manipulation can be predicted by the physical phenotype model of invasion. We previously showed that cancer cells treated with the β-adrenergic agonist, isoproterenol, have increased invasion *in vitro* (14). Activation of β-adrenergic signaling also promotes metastasis in clinically-relevant orthotopic mouse models of breast cancer (46,76). Following treatment of highly metastatic human breast cancer (MDA-MB-231-HM) cells with isoproterenol, we find that E increases from $E_{\text{Control}} = 0.9 \pm 0.4$ kPa to $E_{\text{ISO}} = 4.0 \pm 0.6$ kPa ($p = 0.001$) (Fig. 4C). Similarly, T_T increases from $T_{T\text{ - Control}} = 18 \pm 4.2$ ms to $T_{T\text{ - ISO}} = 81 \pm 31$ ms ($p << 0.001$) (14) (Fig. 4C). While pharmacological perturbation results in altered cell physical phenotypes, the phenotyping model does not accurately predict the effects of isoproterenol on cancer cell invasion (Fig 4F). The inability of the physical phenotyping model to predict the increased invasion caused by this pharmacologic

manipulation suggests that there is a fundamentally different relationship between the effect of β-adrenergic signaling on physical phenotypes and β-adrenergic regulation of invasion compared with the other sets of cancer cells that we investigate here.

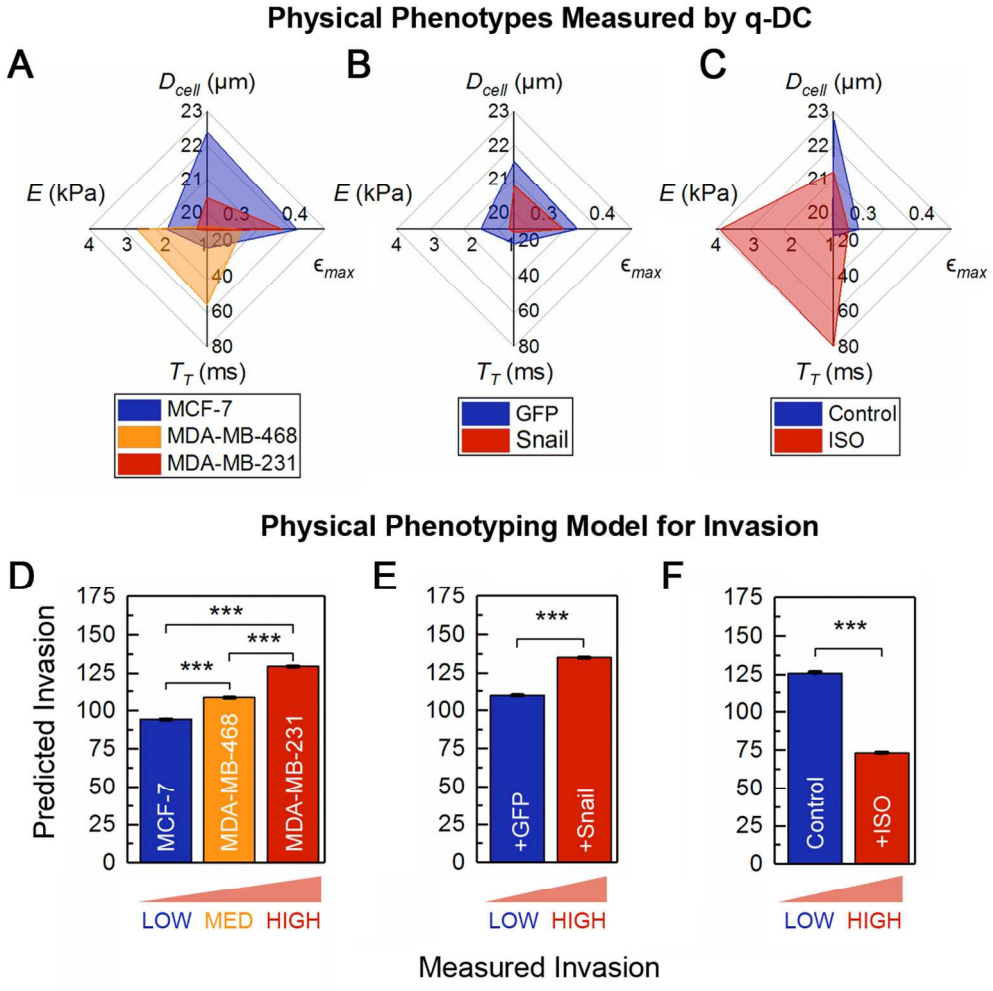

Fig. 4. **Predicting invasion by multiparameter physical phenotyping**. (A-C) The four key physical phenotypes that comprise the reduced set for: (A) breast cancer cells, MCF-7, MDA-MB-468, and MDA-MB-231; (B) ovarian cancer cells, OVCA433-GFP control, and OVCA433 that overexpresses Snail (OVCA433-Snail), a key transcription factor in epithelial-to-mesenchymal transition (EMT); (C) Highly metastatic human breast cancer (MDA-MB-231-HM) cells with activation of β-adrenergic signaling by treatment with 100 nM isoproterenol (+ISO) or vehicle (Control) for 24 h. N > 400. (D-F) Average predicted invasion as determined by the physical phenotyping model for invasion. Error bars represent the standard deviation. Colors represent previously determined invasive potentials, as described in literature (14,55–58).

DISCUSSION

Here we develop the physical phenotyping model to predict invasion using four parameters—elastic modulus E, transit time T_T, maximum strain ϵ_{max}, and cell size D_{cell}—which can be rapidly measured using q-DC. We demonstrate the model's predictive power across ovarian, breast, and pancreatic cell lines that have inherent differences in invasive potential, as well as for cells that have increased invasive potential caused by genetic modification. To generate the physical phenotyping model, we use machine learning methods, which provide a powerful tool to predict clinically relevant phenotypes (25–33). Here we assess invasion, which is used as a metric to determine molecular mediators of metastasis and to validate therapeutic targets in drug discovery (77,78). However, typical invasion assays require hours to days (77,79). The ability to predict cancer cell invasion based on physical phenotyping of single cells within minutes would thus achieve order of magnitude advances in the time required to assess cell invasion; this could enable rapid evaluation of how patient samples, such as cells from pleural effusions or dissociated tumors, respond to drugs.

Physical phenotypes as indicators of invasion. The physical phenotyping model for invasion relies on the reduced set of physical phenotypes—elastic modulus E, transit time T_T, maximum strain ϵ_{max}, and cell size D_{cell}—which can be rapidly measured using q-DC:

Elastic modulus. E is an essential indicator of invasion in the physical phenotype model. Our investigation of physical phenotypes across nineteen cell samples, including established cell lines and a range of genetic and pharmacologic perturbations, provide the opportunity to examine how broadly the relationship between cell stiffness and invasion can be generalized. We find that E is the physical phenotype that is most highly correlated with invasion (S. Fig. 4), reflecting the general trend that more invasive cells tend to be more compliant. Interestingly, we identify several contexts where more invasive cells are stiffer. For example, while overexpression of many of the microRNAs cause ovarian cancer (HEYA8) cells to become stiffer and less invasive, overexpression of microRNA 509-5p causes cells to be stiffer and *more* invasive. We also observe that PANC-1 and Hs766T cells are stiffer and more invasive than MIA PaCa-2 cells. There are additional examples of more invasive cells being stiffer in the breast cancer panel, where MDA-MB-468 cells are stiffer, yet more invasive than MCF-7 cells. Treatment of MDA-MB-231 cells with isoproterenol also causes cells to be stiffer and more invasive. While the overall trend of our data suggests that elastic modulus and invasion are inversely correlated, these and other cases of more invasive cells that are stiffer (13–17), suggest that this inverse correlation is context-dependent.

Transit time. While transit time T_T is commonly used to distinguish cancer cell types (22), this parameter alone is not a strong indicator of invasion. We find moderate to poor association between T_T and invasion across well-characterized cell lines and microRNA-overexpressing cells. The emergence of T_T as an indicator of invasion in the physical phenotyping model suggests that the ability of cells to continuously deform may be important in invasion. While E reflects the ability of a cell to resist initial deformation, and thus dominates viscoelastic response on short millisecond timescales (23), transit time captures the ability of a cell to deform through the entire constriction. We showed previously that T_T depends on both elastic and viscous properties (23); indeed, invasion occurs over hours to days (61), where viscous contributions may be more relevant.

Size. We find that cell size D_{cell} strengthens the accuracy of the physical phenotype model to predict invasion. We and others previously determined that cell size is inversely correlated with

invasion potential (9,44). The effects of cell size may also reflect contributions of the cell nucleus to q-DC measurements: nuclear size scales with cell size (13), and the nucleus tends to be stiffer than the surrounding cytoplasm (11). Moreover, increased nuclear-to-cytoplasmic volume is a hallmark of malignant cells that has diagnostic and prognostic value (2,80,81). Morphological parameters, such as eccentricity and circularity, are also identified as strong predictors of cancer cell types (38); the role of nuclear shape stability in cancer cell physical phenotypes that we investigate here remains to be determined.

This set of physical features $\{E, T_T, D_{cell}, \epsilon_{max}\}$ that we have identified enhances the accuracy of the model to predict cell invasion, but the extent to which they are implicated in invasion is still not fully understood. It is important to emphasize that a biomarker is not required to have a well-established physiological role in order to be an accurate predictor of a disease state. For example, nuclear shape is widely used for cancer prognosis (2–4), but the physiological consequences of aberrant nuclear morphology in cancer cells is still undefined.

Tradeoffs of using multiple physical phenotypes to predict invasion. Our findings demonstrate the enhanced predictive power that can be achieved using multiple physical phenotypes obtained by q-DC, such as elastic modulus E, cell fluidity β, entry time T_E, and maximum strain ϵ_{max} (24). However, extra computation is required to extract these parameters. The tradeoff between model accuracy and computational expense will ultimately depend on the specific application. For example, certain cancer cell populations can be distinguished using measurements of T_T and D_{cell}, which rely on simpler image analysis (10,21–23,59,61). With greater computational investment, such as tracking the time-dependent changes in cell shape during deformation and fitting power law rheology models to the time-dependent strain of single cells, additional parameters such as ϵ_{max} and E can be determined (24). More complex algorithms that exploit the variability of physical phenotypes within cell samples may further improve the accuracy of prediction. However, such enhanced resolution may not be essential for specific applications. For example, the invasion of the epithelial-type OVCA433-GFP cells versus the mesenchymal-type OVCA433-Snail cells is accurately ranked by the median E alone (Fig 4E).

Benefits of q-DC method for machine learning. Since q-DC enables us to obtain calibrated measurements of cell physical phenotypes, this approach addresses the lack of measurement standardization that often challenges the use of machine learning models to predict cellular behaviors (25,26,82,83). Using gel particles as a calibration standard, q-DC enables us to compare data across distinct sets of cell types while avoiding batch-to-batch variation. In addition, the q-DC method enables us to rapidly train the algorithm using a set of cell samples and then evaluate the model performance using a set of seven independent cell samples; this reduces the risk of overfitting by increasing the number of samples compared to the number of measured biomarkers, which is a major challenge in machine learning methods. The ability to rapidly obtain calibrated physical phenotyping data containing multiple features of cells thus provides a powerful complementary biomarker to enrich the feature space available for machine learning approaches.

In contrast to calibrated, physical phenotypes obtained by q-DC, measurements of cell invasion are inherently relative. As the model is evaluated using invasion data from both previous experiments (12–14) and literature (55–58), the predicted invasion cannot be quantitatively compared to the measured invasion. For this reason, we present the assessment of the model's

predictive power as a ranking of invasion of cell types. Future studies that investigate a larger panel of cell types within a single invasion experiment, or compare the invasion of cell types using the same experimental setup, would allow for more detailed evaluation of the accuracy of the predictive model for invasion.

The use of more sophisticated machine learning approaches could further improve performance of the model for invasion. Using stack combinations of machine learning methods can overcome the limitations of individual algorithms and thereby generate a more robust model (84). More advanced algorithms could also minimize the image analysis required for the physical phenotyping model for invasion; for example, neural network algorithms can be trained using images with minimal processing, and thus do not require the additional computational steps to extract physical phenotypes.

Effects of measurement techniques on the physical phenotyping model for invasion. Since different methods for physical phenotyping investigate cells in suspended versus adhered states, it is not clear how broadly the predictors of invasion identified by q-DC can be translated to other physical phenotyping measurements. Microfluidic methods, such as q-DC, probe cells in suspension, where cells exhibit an altered distribution of F-actin compared to when they are adhered to a substrate (13,85). In addition, cells attached to a substrate generate intracellular tension; this 'prestress' (86) can contribute to cell stiffness measurements when using a technique such as AFM (85,87). Considering the increased contractility and/or stress fiber formation of adhered cells may explain the difference in the ranking of elastic modulus values for PDAC cells measured by q-DC and AFM (13). Differences in the time and length scales of mechanical measurements by AFM and q-DC may further contribute to differences in measured physical phenotypes.

Measuring the mechanical properties of cells using complementary methods could provide valuable insight into the role of cell physical phenotypes at varying steps in the metastatic cascade. The stiffness of adhered cells depends on myosin II activity (88–91), which is required for cells to generate forces during invasion, extravasation, and intravasation (92,93); mechanotyping of adhered cells could provide an additional, complementary physical indicator of cell invasion. Indeed, traction stresses scale with cell metastatic potential (94). The ability of suspended cells to deform during circulation through the blood and lymphatic vasculature (92,93) and resist fluid shear stresses (95) is critical for tumor cell dissemination.

The method for measuring cancer cell invasion could also impact the physical phenotyping model for invasion. Results from the 3D scratch wound invasion assay used here are similar to data obtained using a transwell migration assay (13,44). However, the ranking of invasion across cancer cell lines could be influenced by tuning matrix stiffness and/or composition; instead of Matrigel, as used here, collagen or fibronectin, could recapitulate different physiological conditions, where some cell types may be more effective at invading. Since the ability of cells to invade through different matrix materials can differ, the relationship between cell physical phenotypes and invasion should be defined for each context. Such an approach could extend the applicability of this methodology to predict the migration of immune cells or neurons, or wound healing response.

Navigating the physical fitness landscape of invasion. Invasion is a complex and highly dynamic process requiring deformation through micron-scale pores (93,96), protrusion formation (97), generation of traction forces (94), and secretion of proteases (98–100). While we cannot directly conclude from the predictive model that the reduced set of parameters—elastic modulus E, transit time T_T, maximum strain ϵ_{max}, and cell size D_{cell}—contribute to cancer invasion, evidence in the literature suggests that these parameters have functional implications. The stiffness of cells determines their ability to deform through narrow gaps; thus, changes in cell physical properties could have consequences for functional behaviors, such as invasion. Cell size may impact how readily cells can invade through a matrix. Indeed, cell size determines the probability of cells to occlude narrow capillaries or pores (101,102), and thus may be implicated in lodging of cells in metastatic target sites, such as the narrow capillaries of the pulmonary beds of the lung (93). Consistent with these findings, we observe that more invasive cells tend to have lower elastic modulus and smaller cell size (Fig 3B).

While the physical phenotype model predicts the invasion of most contexts we investigate here, the model does not predict the increased invasion of cancer cells with β-adrenergic activation. Specifically, activation of β-adrenergic signaling alters single-cell physical phenotypes and invasion in a way that is not consistent with the other cell samples, including both cell lines and genetically-modified cells. Further studies of how β-adrenergic signaling alters cell physical phenotypes may explain why these cells are stiffer and more invasive, and could facilitate the discovery of additional biomarkers, such as contractility, to predict invasion. For example, the increased stiffness of cells with activation of β-adrenergic signaling requires myosin II activity (14); myosin II is also required for actomyosin contractility, which increases cell stiffness (88–91) and generates forces required for cells to invade through 3D matrices (103,104).

It is intriguing to speculate that different physical phenotype signatures may reflect different strategies for cancer cell invasion. Deeper investigation of contexts where invasion cannot be predicted by the physical phenotype model for invasion may reveal another physical regime that is described by a different set of phenotypes that can predict invasion. Identifying additional complementary biomarkers could generate a more inclusive—even universal—model to predict invasion across varied contexts. Future studies to better elucidate the interplay between physical phenotypes in the invasion 'fitness landscape' will deepen our understanding of potential selective advantages acquired by cancer cells with altered physical phenotypes. In addition, the data that we have generated (SI) should be valuable to for the development of future mechanistic models of cell invasion (105–107), which could provide further insight into the role of these physical phenotypes in regulating invasion.

CONCLUSION

The q-DC method for single-cell physical phenotyping coupled with machine learning algorithms provides an important step towards enhanced classification of cancer cell types. More broadly, the physical phenotyping model provides a framework for understanding and predicting clinically relevant phenotypes. While we define here the relationship between physical phenotypes and invasion, the approach could be extended to investigate other clinically relevant phenotypes, such as sensitivity to chemotherapy agents.

ACKNOWLEDGEMENTS

We are grateful to the National Science Foundation (CAREER DBI-1254185 to ACR), Broad Stem Cell Research Center, UCLA Life Sciences Innovation Fund Award, and the Farber Family Foundation for financial support. We thank Dr. Timothy Donahue (University of California, Los Angeles, USA) for the pancreatic ductal adenocarcinoma cell lines; Dr. Ming-Sound Tsao (University Health Network-Princess Margaret Hospital and University of Toronto, Canada) for the non-transformed human pancreatic ductal epithelial (HPDE) cell line; Dr. Preethi Gunaratne (University of Houston, USA) for the tumor-suppressor microRNAs; and Dr. Ruprecht Wiedemeyer and Dr. Barbie Taylor-Harding (Cedars-Sinai Medical Center, USA) for the OVCA433-GFP and Snail-expressing cell lines. We are also grateful to Massoud Karimzadeh contributed to insightful discussions and to the staff at the Integrated Systems Nanofabrication Cleanroom at the California NanoSystems Institute for supporting the fabrication of the microfluidic devices.

CONFLICT OF INTERESTS

The authors report no conflict of interests.

REFERENCES

1. Brown M, Wittwer C. Flow cytometry: principles and clinical applications in hematology. Clin Chem. United States; 2000 Aug;46(8 Pt 2):1221–9.
2. Elston CW, Ellis IO. Pathological prognostic factors in breast cancer. I. The value of histological grade in breast cancer: experience from a large study with long-term follow-up. Histopathology. England; 1991 Nov;19(5):403–10.
3. Webster M, Witkin KL, Cohen-Fix O. Sizing up the nucleus: nuclear shape, size and nuclear-envelope assembly. J Cell Sci. 2009 May;122(Pt 10):1477–86.
4. Guilak F, Tedrow JR, Burgkart R. Viscoelastic properties of the cell nucleus. Biochem Biophys Res Commun. Elsevier; 2000;269(3):781–6.
5. Guck J, Schinkinger S, Lincoln B, Wottawah F, Ebert S, Romeyke M, et al. Optical deformability as an inherent cell marker for testing malignant transformation and metastatic competence. Biophys J. Elsevier; 2005 May;88(5):3689–98.
6. Cross SE, Jin Y-S, Rao J, Gimzewski JK. Nanomechanical analysis of cells from cancer patients. Nat Nanotechnol. 2007 Dec;2(12):780–3.
7. Hur SC, Henderson-MacLennan NK, McCabe ERB, Di Carlo D. Deformability-based cell classification and enrichment using inertial microfluidics. Lab Chip. England; 2011 Mar;11(5):912–20.
8. Xu W, Mezencev R, Kim B, Wang L, McDonald J, Sulchek T. Cell stiffness is a biomarker of the metastatic potential of ovarian cancer cells. PLoS One. Public Library of Science; 2012;7(10):e46609.
9. Swaminathan V, Mythreye K, O'Brien ET, Berchuck A, Blobe GC, Superfine R. Mechanical stiffness grades metastatic potential in patient tumor cells and in cancer cell lines. Cancer Res. United States; 2011 Aug;71(15):5075–80.
10. Hou HW, Li QS, Lee GYH, Kumar a. P, Ong CN, Lim CT. Deformability study of breast cancer cells using microfluidics. Biomed Microdevices. 2009 Jun;11(3):557–64.
11. Agus DB, Alexander JF, Arap W, Ashili S, Aslan JE, Austin RH, et al. A physical sciences network characterization of non-tumorigenic and metastatic cells. Sci Rep. England; 2013;3:1449.
12. Chan CK, Pan Y, Nyberg K, Marra MA, Lim EL, Jones SJ, et al. Tumour-suppressor microRNAs regulate ovarian cancer cell physical properties and invasive behaviour. Open Biol. 2016;6(11).
13. Nguyen A V, Nyberg KD, Scott MB, Welsh AM, Nguyen AH, Wu N, et al. Stiffness of pancreatic cancer cells is associated with increased invasive potential. Integr Biol. England; 2016 Oct;
14. Kim T-H, Gill NK, Nyberg KD, Nguyen A V, Hohlbauch S V, Geisse NA, et al. Cancer cells become less deformable and more invasive with activation of beta-adrenergic signaling. J Cell Sci. England; 2016 Dec;129(24):4563–75.
15. Liu C-Y, Lin H-H, Tang M-J, Wang Y-K. Vimentin contributes to epithelial-mesenchymal transition cancer cell mechanics by mediating cytoskeletal organization and focal adhesion maturation. Oncotarget. United States; 2015 Jun;6(18):15966–83.
16. Rathje L-SZ, Nordgren N, Pettersson T, Ronnlund D, Widengren J, Aspenstrom P, et al. Oncogenes induce a vimentin filament collapse mediated by HDAC6 that is linked to cell stiffness. Proc Natl Acad Sci U S A. United States; 2014 Jan;111(4):1515–20.
17. Weder G, Hendriks-Balk MC, Smajda R, Rimoldi D, Liley M, Heinzelmann H, et al.

Increased plasticity of the stiffness of melanoma cells correlates with their acquisition of metastatic properties. Nanomedicine. United States; 2014 Jan;10(1):141–8.
18. Darling EM, Di Carlo D. High-Throughput Assessment of Cellular Mechanical Properties. Annu Rev Biomed Eng. United States; 2015;17:35–62.
19. Lange JR, Steinwachs J, Kolb T, Lautscham LA, Harder I, Whyte G, et al. Microconstriction Arrays for High-Throughput Quantitative Measurements of Cell Mechanical Properties. Biophys J. Biophysical Society; 2015;109(1):26–34.
20. Hoelzle DJ, Varghese BA, Chan CK, Rowat AC. A Microfluidic Technique to Probe Cell Deformability. JoVE. 2014;91:e51474–e51474.
21. Byun S, Son S, Amodei D, Cermak N, Shaw J, Kang JH, et al. Characterizing deformability and surface friction of cancer cells. Proc Natl Acad Sci. 2013;110(19):7580–5.
22. Rosenbluth MJ, Lam WA, Fletcher DA. Analyzing cell mechanics in hematologic diseases with microfluidic biophysical flow cytometry. Lab Chip. Royal Society of Chemistry; 2008 Jul;8(7):1062–70.
23. Nyberg KD, Scott MB, Bruce SL, Gopinath AB, Bikos D, Mason TG, et al. The physical origins of transit time measurements for rapid, single cell mechanotyping. Lab Chip. Royal Society of Chemistry; 2016;16(17):3330–9.
24. Nyberg KD, Hu KH, Kleinman SH, Khismatullin DB, Butte MJ, Rowat AC. Quantitative Deformability Cytometry (q-DC): rapid, calibrated measurements of single cell viscoelastic properties. Biophys J. 2017;16(17).
25. Ko J, Baldassano SN, Loh P-L, Kording K, Litt B, Issadore D. Machine learning to detect signatures of disease in liquid biopsies - a user's guide. Lab Chip. England; 2018 Jan;18(3):395–405.
26. Kording KP, Benjamin A, Farhoodi R, Glaser JI. The Roles of Machine Learning in Biomedical Science. In: Frontiers of Engineering: Reports on Leading-Edge Engineering from the 2017 Symposium. 2018.
27. Chen CL, Mahjoubfar A, Tai L-C, Blaby IK, Huang A, Niazi KR, et al. Deep Learning in Label-free Cell Classification. Sci Rep. England; 2016 Mar;6:21471.
28. Agranoff D, Fernandez-Reyes D, Papadopoulos MC, Rojas SA, Herbster M, Loosemore A, et al. Identification of diagnostic markers for tuberculosis by proteomic fingerprinting of serum. Lancet (London, England). England; 2006 Sep;368(9540):1012–21.
29. Varma VR, Oommen AM, Varma S, Casanova R, An Y, Andrews RM, et al. Brain and blood metabolite signatures of pathology and progression in Alzheimer disease: A targeted metabolomics study. PLoS Med. United States; 2018 Jan;15(1):e1002482.
30. Levy B, Hu ZI, Cordova KN, Close S, Lee K, Becker D. Clinical Utility of Liquid Diagnostic Platforms in Non-Small Cell Lung Cancer. Oncologist. United States; 2016 Sep;21(9):1121–30.
31. Burrell RA, McGranahan N, Bartek J, Swanton C. The causes and consequences of genetic heterogeneity in cancer evolution. Nature. England; 2013 Sep;501(7467):338–45.
32. Crowley E, Di Nicolantonio F, Loupakis F, Bardelli A. Liquid biopsy: monitoring cancer-genetics in the blood. Nat Rev Clin Oncol. England; 2013 Aug;10(8):472–84.
33. Fu Q, Schoenhoff FS, Savage WJ, Zhang P, Van Eyk JE. Multiplex assays for biomarker research and clinical application: translational science coming of age. Proteomics Clin Appl. Germany; 2010 Mar;4(3):271–84.
34. Lee WC, Shi H, Poon Z, Nyan LM, Kaushik T, Shivashankar G V, et al. Multivariate

biophysical markers predictive of mesenchymal stromal cell multipotency. Proc Natl Acad Sci. United States; 2014 Oct;111(42):E4409-18.
35. Bongiorno T, Chojnowski JL, Lauderdale JD, Sulchek T. Cellular Stiffness as a Novel Stemness Marker in the Corneal Limbus. Biophys J. United States; 2016 Oct;111(8):1761–72.
36. Bongiorno T, Kazlow J, Mezencev R, Griffiths S, Olivares-Navarrete R, McDonald JF, et al. Mechanical stiffness as an improved single-cell indicator of osteoblastic human mesenchymal stem cell differentiation. J Biomech. Elsevier; 2014;47(9):2197–204.
37. Gossett DR, Tse HTK, Lee S a., Ying Y, Lindgren AG, Yang OO, et al. Hydrodynamic stretching of single cells for large population mechanical phenotyping. Proc Natl Acad Sci. National Acad Sciences; 2012 May;109(20):7630–5.
38. Lin J, Kim D, Henry TT, Tseng P, Peng L, Dhar M, et al. High-throughput physical phenotyping of cell differentiation. Microsystems Nanoeng. Nature Publishing Group; 2017;3:17013.
39. Darling EM, Topel M, Zauscher S, Vail TP, Guilak F. Viscoelastic properties of human mesenchymally-derived stem cells and primary osteoblasts, chondrocytes, and adipocytes. J Biomech. United States; 2008;41(2):454–64.
40. Darling EM, Guilak F. A neural network model for cell classification based on single-cell biomechanical properties. Tissue Eng Part A. United States; 2008 Sep;14(9):1507–15.
41. Tse HTK, Gossett DR, Moon YS, Masaeli M, Sohsman M, Ying Y, et al. Quantitative diagnosis of malignant pleural effusions by single-cell mechanophenotyping. Sci Transl Med. United States; 2013 Nov;5(212):212ra163.
42. Jiang Y, Lei C, Yasumoto A, Kobayashi H, Aisaka Y, Ito T, et al. Label-free detection of aggregated platelets in blood by machine-learning-aided optofluidic time-stretch microscopy. Lab Chip. England; 2017 Jul;17(14):2426–34.
43. Pan Y, Robertson G, Pedersen L, Lim E, Hernandez-Herrera A, Rowat AC, et al. miR-509-3p is clinically significant and strongly attenuates cellular migration and multi-cellular spheroids in ovarian cancer. Oncotarget. United States; 2016 May;7(18):25930–48.
44. Chan CK, Pan Y, Nyberg K, Marra MA, Lim EL, Jones SJM, et al. Tumour-suppressor microRNAs regulate ovarian cancer cell physical properties and invasive behaviour. Open Biol. England; 2016 Nov;6(11).
45. Qi D, Gill NK, Santiskulvong C, Sifuentes J, Dorigo O, Rao J, et al. Screening cell mechanotype by parallel microfiltration. Sci Rep. Nature Publishing Group; 2015;5.
46. Le CP, Nowell CJ, Kim-Fuchs C, Botteri E, Hiller JG, Ismail H, et al. Chronic stress in mice remodels lymph vasculature to promote tumour cell dissemination. Nat Commun. England; 2016 Mar;7:10634.
47. Duffy DC, McDonald JC, Schueller OJA, Whitesides GM. Rapid prototyping of microfluidic systems in poly(dimethylsiloxane). Anal Chem. 1998 Dec;70(23):4974–84.
48. Eddington DT, Crone WC, Beebe DJ. Development of process protocols to fine tune polydimethylsiloxane material properties. In: 7th International Conference on Miniaturized Chemical and Biochemical Analysis Systems. 2003. p. 1089–92.
49. Byun S, Son S, Amodei D, Cermak N, Shaw J, Ho J, et al. Characterizing deformability and surface friction of cancer cells. 2013;
50. Shaw Bagnall J, Byun S, Begum S, Miyamoto DT, Hecht VC, Maheswaran S, et al. Deformability of Tumor Cells versus Blood Cells. Sci Rep. England; 2015;5:18542.

51. Nyberg KD, Scott MB, Bruce SL, Gopinath AB, Bikos D, Mason TG, et al. The physical origins of transit time measurements for rapid, single cell mechanotyping. Lab Chip. 2016;16(17).
52. Beyer K, Goldstein J, Ramakrishnan R, Shaft U. When is "nearest neighbor" meaningful? In: International conference on database theory. Springer; 1999. p. 217–35.
53. Hall P, Park BU, Samworth RJ. Choice of neighbor order in nearest-neighbor classification. Ann Stat. JSTOR; 2008;2135–52.
54. Hassanat AB, Abbadi MA, Altarawneh GA, Alhasanat AA. Solving the problem of the K parameter in the KNN classifier using an ensemble learning approach. arXiv Prepr arXiv14090919. 2014;
55. Gordon LA, Mulligan KT, Maxwell-Jones H, Adams M, Walker RA, Jones JL. Breast cell invasive potential relates to the myoepithelial phenotype. Int J cancer. Wiley Online Library; 2003;106(1):8–16.
56. Albini A, Iwamoto Y, Kleinman HK, Martin GR, Aaronson SA, Kozlowski JM, et al. A rapid in vitro assay for quantitating the invasive potential of tumor cells. Cancer Res. United States; 1987 Jun;47(12):3239–45.
57. Sheridan C, Kishimoto H, Fuchs RK, Mehrotra S, Bhat-Nakshatri P, Turner CH, et al. CD44+/CD24- breast cancer cells exhibit enhanced invasive properties: an early step necessary for metastasis. Breast Cancer Res. England; 2006;8(5):R59.
58. Chekhun S, Bezdenezhnykh N, Shvets J, Lukianova N. Expression of biomarkers related to cell adhesion, metastasis and invasion of breast cancer cell lines of different molecular subtype. Exp Oncol. Ukraine; 2013 Sep;35(3):174–9.
59. Rowat AC, Jaalouk DE, Zwerger M, Ung WL, Eydelnant IA, Olins DE, et al. Nuclear Envelope Composition Determines the Ability of Neutrophil-type Cells to Passage through Micron-scale Constrictions. J Biol Chem. 2013 Mar;288(12):8610–8.
60. Lange JR, Metzner C, Richter S, Schneider W, Spermann M, Kolb T, et al. Unbiased High-Precision Cell Mechanical Measurements with Microconstrictions. Biophys J. Elsevier; 2017;112(7):1472–80.
61. Ekpenyong AE, Whyte G, Chalut K, Pagliara S, Lautenschläger F, Fiddler C, et al. Viscoelastic Properties of Differentiating Blood Cells Are Fate- and Function-Dependent. PLoS One. 2012;7(9).
62. Nguyen AV, Nyberg KD, Scott MB, Welsh AM, Nguyen AH, Wu N, et al. Stiffness of pancreatic cancer cells is associated with increased invasive potential. Integr Biol (United Kingdom). 2016;8(12).
63. Soltani M, Vargas-Garcia CA, Antunes D, Singh A. Intercellular Variability in Protein Levels from Stochastic Expression and Noisy Cell Cycle Processes. PLoS Comput Biol. United States; 2016 Aug;12(8):e1004972.
64. Gabriele S, Benoliel AM, Bongrand P, Théodoly O. Microfluidic investigation reveals distinct roles for actin cytoskeleton and myosin II activity in capillary leukocyte trafficking. Biophys J. Biophysical Society; 2009;96(10):4308–18.
65. Rosenbluth MJ, Lam WA, Fletcher DA. Force microscopy of nonadherent cells: a comparison of leukemia cell deformability. Biophys J. 2006;90:2994–3003.
66. Otto O, Rosendahl P, Mietke A, Golfier S, Herold C, Klaue D, et al. Real-time deformability cytometry: on-the-fly cell mechanical phenotyping. Nat Methods. 2015;12(3).
67. Needham D, Hochmuth RM. Rapid flow of passive neutrophils into a 4 microns pipet and

measurement of cytoplasmic viscosity. J Biomech Eng. 1990;112:269–76.
68. Tsai MA, Waugh RE, Keng PC. Cell cycle-dependence of HL-60 cell deformability. Biophys J. Elsevier; 1996;70(4):2023–9.
69. Pajerowski JD, Dahl KN, Zhong FL, Sammak PJ, Discher DE. Physical plasticity of the nucleus in stem cell differentiation. Proc Natl Acad Sci. 2007;104(40):15619–24.
70. Fabry B, Maksym GN, Butler JP, Glogauer M, Navajas D, Fredberg JJ. Scaling the microrheology of living cells. Phys Rev Lett. APS; 2001;87(14):148102.
71. Krijthe J, van der Maaten L. T-Distributed Stochastic Neighbor Embedding using a Barnes-Hut Implementation [Internet]. Vienna, Austria: R Foundation for Statistical Computing; 2017. Available from: https://github.com/jkrijthe/Rtsne
72. Adams M, Jones JL, Walker RA, Pringle JH, Bell SC. Changes in tenascin-C isoform expression in invasive and preinvasive breast disease. Cancer Res. United States; 2002 Jun;62(11):3289–97.
73. De Craene B, Gilbert B, Stove C, Bruyneel E, van Roy F, Berx G. The transcription factor snail induces tumor cell invasion through modulation of the epithelial cell differentiation program. Cancer Res. United States; 2005 Jul;65(14):6237–44.
74. Behrens J, Mareel MM, Van Roy FM, Birchmeier W. Dissecting tumor cell invasion: epithelial cells acquire invasive properties after the loss of uvomorulin-mediated cell-cell adhesion. J Cell Biol. United States; 1989 Jun;108(6):2435–47.
75. Guadamillas MC, Cerezo A, Del Pozo MA. Overcoming anoikis--pathways to anchorage-independent growth in cancer. J Cell Sci. England; 2011 Oct;124(Pt 19):3189–97.
76. Creed SJ, Le CP, Hassan M, Pon CK, Albold S, Chan KT, et al. beta2-adrenoceptor signaling regulates invadopodia formation to enhance tumor cell invasion. Breast Cancer Res. England; 2015 Nov;17(1):145.
77. Hulkower KI, Herber RL. Cell Migration and Invasion Assays as Tools for Drug Discovery. Pharmaceutics [Internet]. MDPI; 2011 Mar 11;3(1):107–24. Available from: http://www.ncbi.nlm.nih.gov/pmc/articles/PMC3857040/
78. Eccles SA, Box C, Court W. Cell migration/invasion assays and their application in cancer drug discovery. Biotechnol Annu Rev. Netherlands; 2005;11:391–421.
79. Kramer N, Walzl A, Unger C, Rosner M, Krupitza G, Hengstschlager M, et al. In vitro cell migration and invasion assays. Mutat Res. Netherlands; 2013;752(1):10–24.
80. Johnston DG. Cytoplasmic:nuclear ratios in the cytological diagnosis of cancer. Cancer. United States; 1952 Sep;5(5):945–9.
81. Foraker AG, Reagan JW. Nuclear size and nuclear: cytoplasmic ratio in the delineation of atypical hyperplasia of the uterine cervix. Cancer. United States; 1956;9(3):470–9.
82. Vidyasagar M. Identifying predictive features in drug response using machine learning: opportunities and challenges. Annu Rev Pharmacol Toxicol. United States; 2015;55:15–34.
83. Abu-Mostafa YS, Magdon-Ismail M, Lin H-T. Learning from data. Vol. 4. AMLBook New York, NY, USA:; 2012.
84. Ko J, Bhagwat N, Yee SS, Ortiz N, Sahmoud A, Black T, et al. Combining Machine Learning and Nanofluidic Technology To Diagnose Pancreatic Cancer Using Exosomes. ACS Nano. United States; 2017 Nov;11(11):11182–93.
85. Maloney JM, Nikova D, Lautenschläger F, Clarke E, Langer R, Guck J, et al. Mesenchymal stem cell mechanics from the attached to the suspended state. Biophys J. Elsevier; 2010;99(8):2479–87.

86. Gardel ML, Nakamura F, Hartwig JH, Crocker JC, Stossel TP, Weitz DA. Prestressed F-actin networks cross-linked by hinged filamins replicate mechanical properties of cells. Proc Natl Acad Sci. United States; 2006 Feb;103(6):1762–7.
87. Rotsch C, Radmacher M. Drug-induced changes of cytoskeletal structure and mechanics in fibroblasts: an atomic force microscopy study. Biophys J. Elsevier; 2000;78(1):520–35.
88. Martens JC, Radmacher M. Softening of the actin cytoskeleton by inhibition of myosin II. Pflugers Arch Eur J Physiol. Springer; 2008;456(1):95–100.
89. Murrell M, Oakes PW, Lenz M, Gardel ML. Forcing cells into shape: the mechanics of actomyosin contractility. Nat Rev Mol Cell Biol. England; 2015 Aug;16(8):486–98.
90. Wang N, Naruse K, Stamenovic D, Fredberg JJ, Mijailovich SM, Tolic-Norrelykke IM, et al. Mechanical behavior in living cells consistent with the tensegrity model. Proc Natl Acad Sci U S A. United States; 2001 Jul;98(14):7765–70.
91. Wang N, Tolic-Norrelykke IM, Chen J, Mijailovich SM, Butler JP, Fredberg JJ, et al. Cell prestress. I. Stiffness and prestress are closely associated in adherent contractile cells. Am J Physiol Cell Physiol. United States; 2002 Mar;282(3):C606-16.
92. Chambers AF, Groom AC, MacDonald IC. Dissemination and growth of cancer cells in metastatic sites. Nat Rev Cancer. England; 2002 Aug;2(8):563–72.
93. Wirtz D, Konstantopoulos K, Searson PC. The physics of cancer: the role of physical interactions and mechanical forces in metastasis. Nat Rev Cancer. England; 2011 Jun;11(7):512–22.
94. Kraning-Rush CM, Califano JP, Reinhart-King CA. Cellular traction stresses increase with increasing metastatic potential. PLoS One. United States; 2012;7(2):e32572.
95. Barnes JM, Nauseef JT, Henry MD. Resistance to fluid shear stress is a conserved biophysical property of malignant cells. PLoS One. United States; 2012;7(12):e50973.
96. Denais CM, Gilbert RM, Isermann P, McGregor AL, te Lindert M, Weigelin B, et al. Nuclear envelope rupture and repair during cancer cell migration. Science. United States; 2016 Apr;352(6283):353–8.
97. Olson MF, Sahai E. The actin cytoskeleton in cancer cell motility. Clin Exp Metastasis. Netherlands; 2009;26(4):273–87.
98. Ma C, Wu B, Huang X, Yuan Z, Nong K, Dong B, et al. SUMO-specific protease 1 regulates pancreatic cancer cell proliferation and invasion by targeting MMP-9. Tumour Biol. United States; 2014 Dec;35(12):12729–35.
99. Zhao X, Gao S, Ren H, Sun W, Zhang H, Sun J, et al. Hypoxia-inducible factor-1 promotes pancreatic ductal adenocarcinoma invasion and metastasis by activating transcription of the actin-bundling protein fascin. Cancer Res. United States; 2014 May;74(9):2455–64.
100. Nabeshima K, Inoue T, Shimao Y, Sameshima T. Matrix metalloproteinases in tumor invasion: role for cell migration. Pathol Int. Australia; 2002 Apr;52(4):255–64.
101. Doerschuk CM, Beyers N, Coxson HO, Wiggs B, Hogg JC. Comparison of neutrophil and capillary diameters and their relation to neutrophil sequestration in the lung. J Appl Physiol. United States; 1993 Jun;74(6):3040–5.
102. Bathe M, Shirai A, Doerschuk CM, Kamm RD. Neutrophil transit times through pulmonary capillaries: the effects of capillary geometry and fMLP-stimulation. Biophys J. Elsevier; 2002;83(4):1917–33.
103. Poincloux R, Collin O, Lizarraga F, Romao M, Debray M, Piel M, et al. Contractility of the cell rear drives invasion of breast tumor cells in 3D Matrigel. Proc Natl Acad Sci U S

A. United States; 2011 Feb;108(5):1943–8.
104. Petrie RJ, Koo H, Yamada KM. Generation of compartmentalized pressure by a nuclear piston governs cell motility in a 3D matrix. Science. United States; 2014 Aug;345(6200):1062–5.
105. Katira P, Bonnecaze RT, Zaman MH. Modeling the mechanics of cancer: effect of changes in cellular and extra-cellular mechanical properties. Front Oncol. Switzerland; 2013;3:145.
106. Katira P, Zaman MH, Bonnecaze RT. How changes in cell mechanical properties induce cancerous behavior. Phys Rev Lett. United States; 2012 Jan;108(2):28103.
107. Danuser G, Allard J, Mogilner A. Mathematical modeling of eukaryotic cell migration: insights beyond experiments. Annu Rev Cell Dev Biol. United States; 2013;29:501–28.

Table of Contents Entry

High throughput quantitative deformability cytometry (q-DC) is used to develop a predictive model of cancer cell invasion based on physical phenotypes.